CRYSTAL GROWTH & DESIGN
2008
VOL. 8, NO. 6
1818–1822

Synthesis and Photoluminescence of Si-Related Nanowires Using Porous Silicon as Si Element Source

Yajun Yang,[†] Guowen Meng,*[,†] Xianyun Liu,[‡] Xiaoguang Zhu,[†] Mingguang Kong,[†] Fangming Han,[†] Xianglong Zhao,[†] Qiaoling Xu,[†] and Lide Zhang[†]

Key Laboratory of Materials Physics, and Anhui Key Laboratory of Nanomaterials and Nanostructures, Institute of Solid State Physics, Chinese Academy of Sciences, Hefei, 230031, China, and Laboratory of Environmental Spectroscopy, Anhui Institute of Optics and Fine Mechanics, Chinese Academy of Sciences, Hefei, 230031, China

Received March 17, 2008; Revised Manuscript Received April 15, 2008

ABSTRACT: Compound nanowires (NWs) of Si-related materials, such as SiC, Si_3N_4, and Zn_2SiO_4 have been synthesized in high yield via a simple thermal evaporation, chemical reaction, and deposition process using porous silicon as the Si element source. The vapor-solid growth mechanism of NWs plays a main role in the formation of the as-prepared Si-related NWs. Photoluminescence (PL) measurements reveal that SiC NWs emit an ultraviolet light at 364 nm, Si_3N_4 NWs shows a broad PL spectrum with a maximum at 495 nm, and Zn_2SiO_4 NWs reveals a green emission at about 510 nm. These Si-related NWs have potential in both composites and optoelectronic nanodevices.

1. Introduction

. One-dimensional (1D) nanostructured materials containing silicon, such as silicon carbide (SiC) nanowires (NWs),[1–7] silicon nitride (Si_3N_4) NWs,[8–11] and zinc silicate (Zn_2SiO_4) NWs,[12,13] have received much attention due to their distinct physical and chemical performances. SiC[1–4] and Si_3N_4[10,11] NWs have potential applications in electronic and optic nanodevices in harsh conditions (high temperature, high frequency, or high power) owing to their fine mechanical properties, low density, superplasticity, good resistance to thermal shock and oxidation, and high fracture toughness. Zn_2SiO_4 NWs may have potential in future gas sensor and optoelectronic nanodevices.[12,13] For the synthesis of these Si-related NWs, Si powder,[1,2,9] SiO,[10,14,15] SiO_2,[3,16,17] and Si wafer,[12,13,18] are usually used as the elemental Si source. Here we demonstrate a generic synthesis of these Si-related NWs, through a simple thermal evaporation, chemical reaction, and deposition process using porous silicon (PS) wafer as the Si source. Compared with other previously used Si source materials, it is much easier to achieve vaporous species Si from PS via evaporation due to its large specific surface area for its nano and porous structures. By using our current method, a high yield of SiC, Si_3N_4, and Zn_2SiO_4 NWs has been achieved without introducing impurities. The method might also be exploited to fabricate other Si-related NWs.

2. Experimental Section

2.1. Synthesis of PS Film. PS film was obtained by electrochemical etching monocrystalline p-type silicon (100) substrate (Boron doped, 8−15 Ω cm) at 20 mA/cm^2 for 30 min, in a 1:1 (v/v) mixture of aqueous HF (49% hydrofluoric acid) and ethanol.[19]

2.2. Synthesis of SiC NWs. The homemade PS film loaded in a ceramic boat was put into the hot zone of a horizontal tubular furnace. The system was heated up to 1350 °C in 15 min, and held at this temperature for 2 h. Ethanol was used as the carbon source in our experiment. A constant gas flow of Ar (purity: 99.999%) went through the ethanol at a flow rate of 30 sccm and was maintained during both the heating and cooling process. After the reaction was terminated and the furnace was cooled to room temperature, the products were exposed to air and heated at 600 °C for about 4 h to remove the superfluous carbon. Finally, wool-like products were found on the half-surface of the ceramic boat located in the downstream.

2.3. Synthesis of Si_3N_4 NWs. The synthesis process is similar to that of SiC. The system was heated up to 1250 °C in 15 min, and held at this temperature for 4 h. A constant mixture gas flow of NH_3 (purity: 99.999%, at a flow rate of 50 sccm) and Ar (purity: 99.999%, at a rate of 30 sccm) was maintained during both the heating and the cooling stages. After the system was cooled down to room temperature, wool-like products were produced on the half-surface of the ceramic boat in the downstream.

2.4. Synthesis of Zn_2SiO_4 NWs. Zn powder (0.1 g, purity: 99%) loaded in a ceramic boat was put into the hot zone of a horizontal tubular furnace. Home-made PS film was placed downstream of the source material at a distance of about 6 cm. The system was heated up to 1200 °C in 15 min, and held at this temperature for 2 h. A constant gas flow of Ar/O_2 (9:1) mixture was kept at 50 sccm during both the heating and cooling process. After the reaction, white products were achieved on the whole surface of the PS wafer.

2.5. Characterization of the NWs. The resulting products were characterized by X-ray diffraction (XRD, X'Pert Pro MPD), scanning electron microscopy (SEM, Sirion 200), and transmission electron microscopy (TEM, JEOL 2010). Photoluminescence (PL) spectra of the products were recorded on spectroscopy (Edinburgh luminescence spectrometer FLS 920, excitation source: Xe lamp).

3. Results and Discussion

3.1. β-SiC NWs Achieved via Evaporating and Carbonizing Porous Silicon. Figure 1a shows the X-ray diffraction (XRD) pattern of the resulting SiC products. All of the strong intensity peaks can be indexed to β-SiC (JCPDS 29-1129). Figure 1b is a scanning electron microscopy (SEM) image of the SiC NWs, and the inset is a close-up view, revealing that the products are a high yield of NWs of tens of micrometers long and 100−400 nm in diameter. Transmission electron microscopy (TEM) observation reveals that there exist three types of SiC NWs sheathed with amorphous SiO_x as shown in Figure 1c−e. Figure 1c is a coaxial SiO_x sheathed β-SiC NW with a diameter of about 100 nm, and the inset is a typical selected area electron diffraction (SAED) pattern of this NW. The inner crystalline SiC NW core has a κ growth direction. The streaks in the SAED pattern are due to the dense stacking faults and microtwins along the κ direction.[2] Figure 1d is another kind of coaxial SiO_x sheathed β-SiC NW with its SAED pattern, displaying periodic structural morphology with a κ growth direction. It seems that the NW is formed by a row of inlaid

* Corresponding author. E-mail: gwmeng@issp.ac.cn.
† Institute of Solid State Physics.
‡ Anhui Institute of Optics and Fine Mechanics.

10.1021/cg800284u CCC: $40.75 © 2008 American Chemical Society
Published on Web 05/07/2008

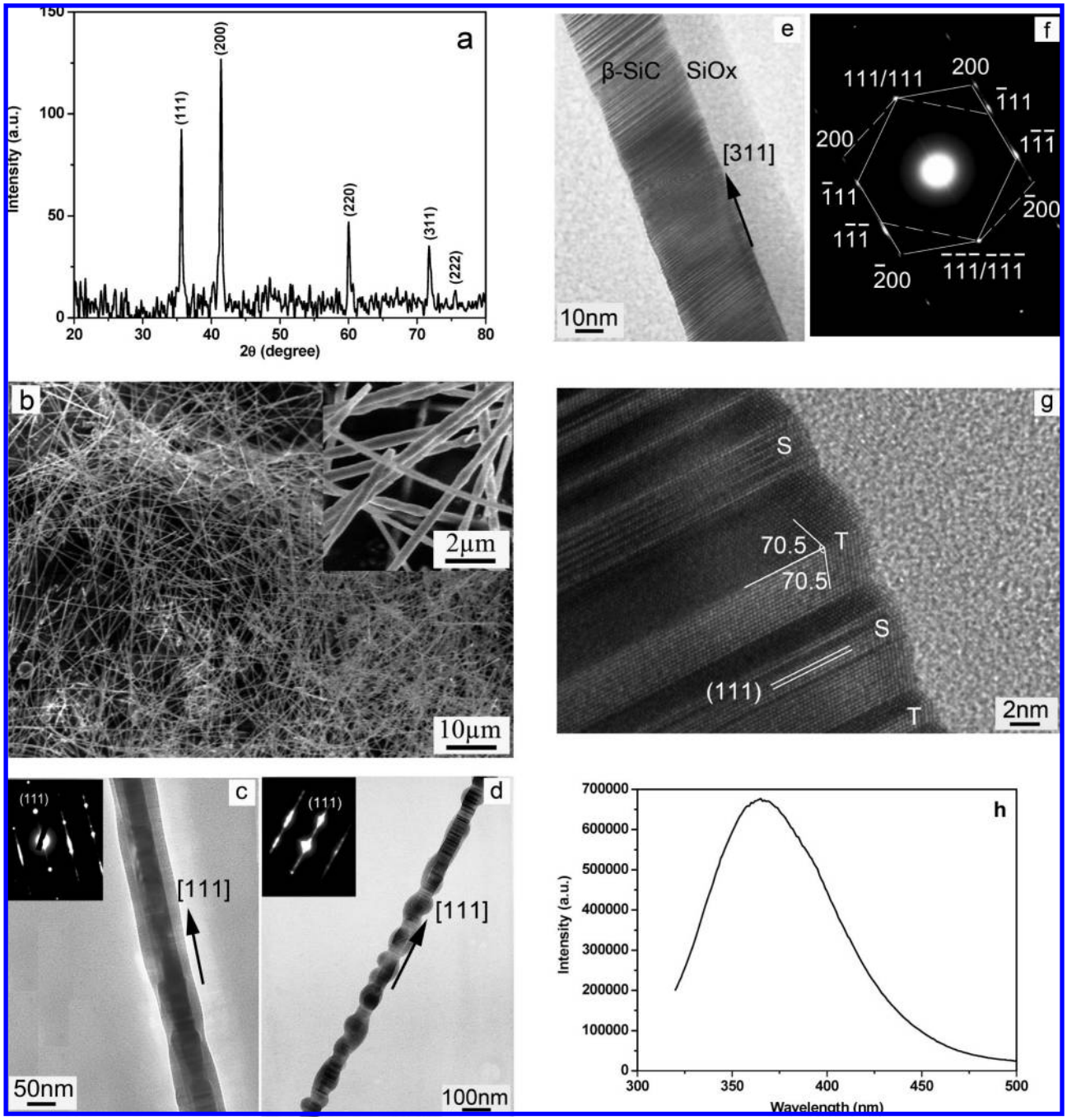

Figure 1. (a) XRD pattern of the SiC NWs. (b) SEM image of the SiC NWs. The upper-right is a magnified image. (c) TEM image of a coaxially SiO_x sheathed β-SiC NW. (d) TEM image of another kind of coaxially structured β-SiC NW. (e) TEM image of a biaxially structured β-SiC NW. (f) SAED pattern from SiC NW in the biaxially structured SiC-SiO_x NW. (g) Lattice-resolved image of enlargement of the SiC-SiO_x interface. S and T stand for stacking fault and twin, respectively. (h) Room-temperature PL spectrum from the β-SiC NWs wrapped with an amorphous SiO_x sheath.

SiO_x along the axis of the SiC NW. Although the thickness of the SiO_x sheath varies, the diameter of the SiC NW core is uniform along the NW. Figure 1e shows a SiO_x sheathed biaxial β-SiC NW consisting of two side-by-side sub-NWs of amorphous silica and crystalline β-SiC with [311] orientation, which can be also referred to as a composite NW.[20] The side crystalline β-SiC NW has a high density of stacking faults and microtwins. Figure 1f is the SAED pattern taken along the [01$\bar{1}$] zone axis, perpendicular to this NW, indicating the existence of a twin defect along the [111] direction. The stacking faults and twins can be seen clearly in an enlargement of a local region (Figure 1g), where the outermost surface of the β-SiC NW is composed of {111} facets. The zigzag angles are about 141° (70.5° + 70.5°), in accordance with the relative rotational angle of (111) twin crystals in face-centered (fcc) structures.[21] Twin crystals along {111} facets in fcc structures are occasionally observed due to their crystallographic characteristics.[21]

To explain the growth mechanism for crystalline NWs, several models including vapor−solid (VS) and vapor−liquid−solid (VLS) mechanisms have been proposed.[18] The main feature of the VLS mechanism is the presence of intermediates that serve as catalysts between the vapor feed and the solid growth at elevated temperature, and the morphology feature is a catalyst ball on the end of the NW.[3] However, the VLS mechanism seems not to be the case in this work, because there are not any droplets observed on the ends of the NWs. In addition, the only source material used in the experiment is a pure PS wafer. Therefore, the growth mechanism

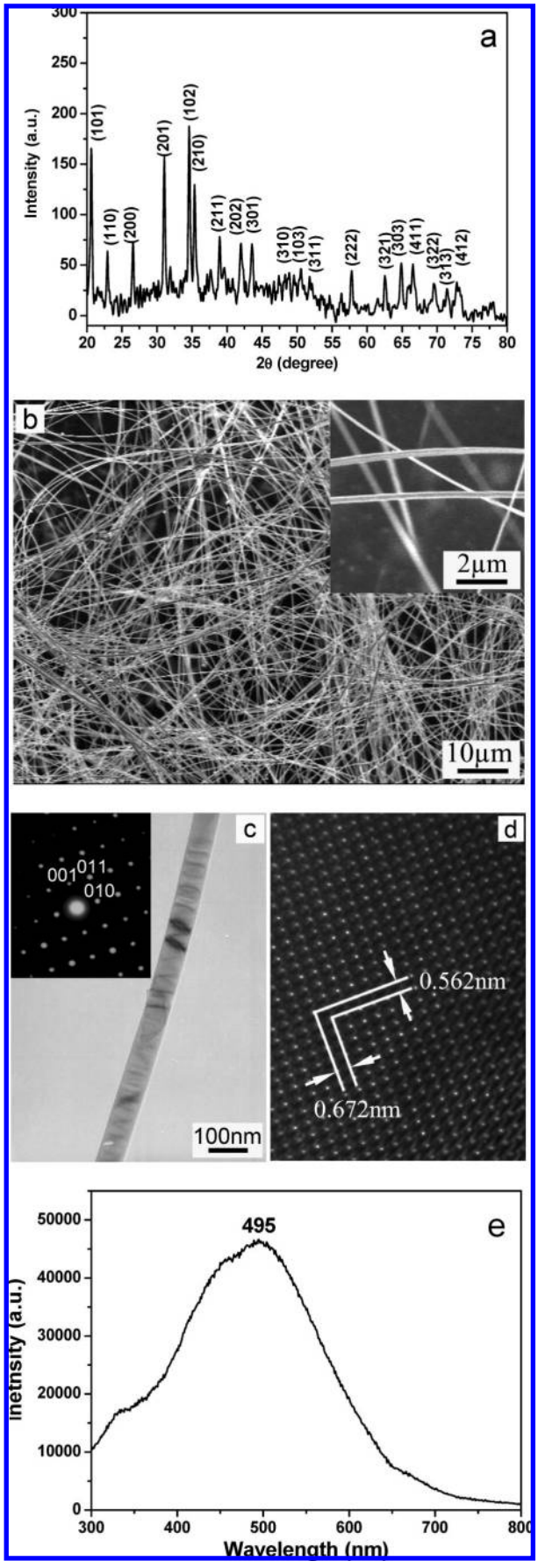

Figure 2. (a) XRD pattern of the α-Si_3N_4 NWs. (b) SEM image of the α-Si_3N_4 NWs. The inset shows a magnified image. (c) TEM image and SAED pattern (inset) of a typical α-Si_3N_4 NW. (d) Its corresponding HRTEM image. (e) Room-temperature PL spectrum from the α-Si_3N_4 NWs.

of the SiC NWs might be a VS process that can be described as follows. At the heating temperature of 1350 °C, Si vaporous species is evaporated from the PS wafer with a high specific surface area, and reacts with active carbon species decomposed from C_2H_5OH. The resultant SiC molecules are transported to the downstream side of PS wafer on the ceramic boat by the carrier gas (Ar) and then land on the surface of ceramic boat as SiC nanoparticles, serving as the nuclei of the SiC NWs. As the reaction goes on, more SiC molecules will be generated, and the newly formed SiC molecules will deposit on the SiC nuclei and then form SiC NWs at specific temperature zones, being similar to the formation of SiC NWs from electrospun nanofiber templates.[3] The unique structure of the NWs is likely determined by growth kinetics.[20] It is apparent that oxygen is involved in the growth of biaxial and coaxial nanocables with SiC NWs as cores. The oxygen probably comes from the oxide layer of the PS wafer, because the PS surface is $Si-H_x$-terminated and metastable, and will commence oxidation in air under room light in a few minutes.[22–24] Moreover, oxygen might also come from the residual oxygen in the reaction chamber, or the leakage of heating system.[25] The atomic scale kinks and ledges may increase the surface energy of the SiC NWs. Thus, to minimize the surface energy, oxide layer is likely to form on the surface of SiC NWs, as reported previously.[20]

Room-temperature photoluminescence (PL) spectrum (Figure 1h) of the β-SiC NWs with SiO_x sheath has been measured using an excitation wavelength of 300 nm, revealing an ultraviolet emission at 364 nm (3.4 eV). Similar ultraviolet peaks located at 355 and 370 nm were observed for SiO_2 powder and thermally oxidized PS.[26] As the SiC NWs with both biaxial and coaxial SiO_x sheath consist of amorphous SiO_x subnanowire or sheath, the ultraviolet peak at 364 nm might be ascribed to the radiative recombination from excess oxygen defects of SiO_x sheath.

3.2. α-Si_3N_4 NWs Achieved via Evaporating and Nitridizing Porous Silicon. Figure 2a is a typical XRD pattern of the Si_3N_4 products. All peaks can be indexed to the hexagonal α-Si_3N_4 (JCPDS 41-0360). The strong and sharp reflection peaks suggest that the Si_3N_4 products are well crystallized. Figure 2b is an SEM image of the products, showing large quantities of Si_3N_4 NWs. The inset is a closed-up view, revealing that the Si_3N_4 NWs are 80−200 nm in diameter with lengths of about tens of micrometers. Figure 2c is a TEM image of a single Si_3N_4 NW with its SAED pattern taken from the [100] zone axis. Lattice-resolved image (Figure 2d) of this NW reveals that the Si_3N_4 NW is single crystal with regular spacings of lattice planes of 0.562 and 0.672 nm, corresponding to (001) and (010) crystalline planes of the α-Si_3N_4, respectively. Therefore, the Si_3N_4 NW grows along the [011] direction.

The formation of the Si_3N_4 NWs is similar to that of SiC NWs. At the heating temperature of 1250 °C, Si vapor evaporated from the PS wafer is transported to the downstream by carrier gas Ar. Subsequently, the following chemical reaction of Si vapor and NH_3 takes place:

$$3Si(g) + 4NH_3(g) \rightarrow \alpha\text{-}Si_3N_4(s) + 6H_2(g) \quad (1)$$

Here, g and s refer to gas and solid state, respectively. Then Si_3N_4 molecules deposit on the surface of the ceramic boat in the downstream, resulting in the formation of Si_3N_4 NWs via VS mechanism at specific temperature zones.[18]

Room-temperature PL spectrum (Figure 2e) of the α-Si_3N_4 NWs reveals a broad peak with a maximum centered at 495 nm. Zhou et al.[27] have reported that Si_3N_4 NWs shows a broad PL spectrum with a maximum at 525 nm, which may be caused by the defects. Yin et al.[28] have reported that the PL spectrum of the α-Si_3N_4 nanobelts exhibits an intense and broad spectrum ranging from 420 to 750 nm with a maximum centered at 575 nm (2.16 eV), which is related to the inherent imperfect Si and N dangling bonds in the α-Si_3N_4. Mo et al.[29] have reported luminescence of nanometer-sized amorphous Si_3N_4 solids. Nanometer-sized amorphous Si_3N_4 has defect energy levels, such as ≡Si−Si≡ (the Si−Si energy level),

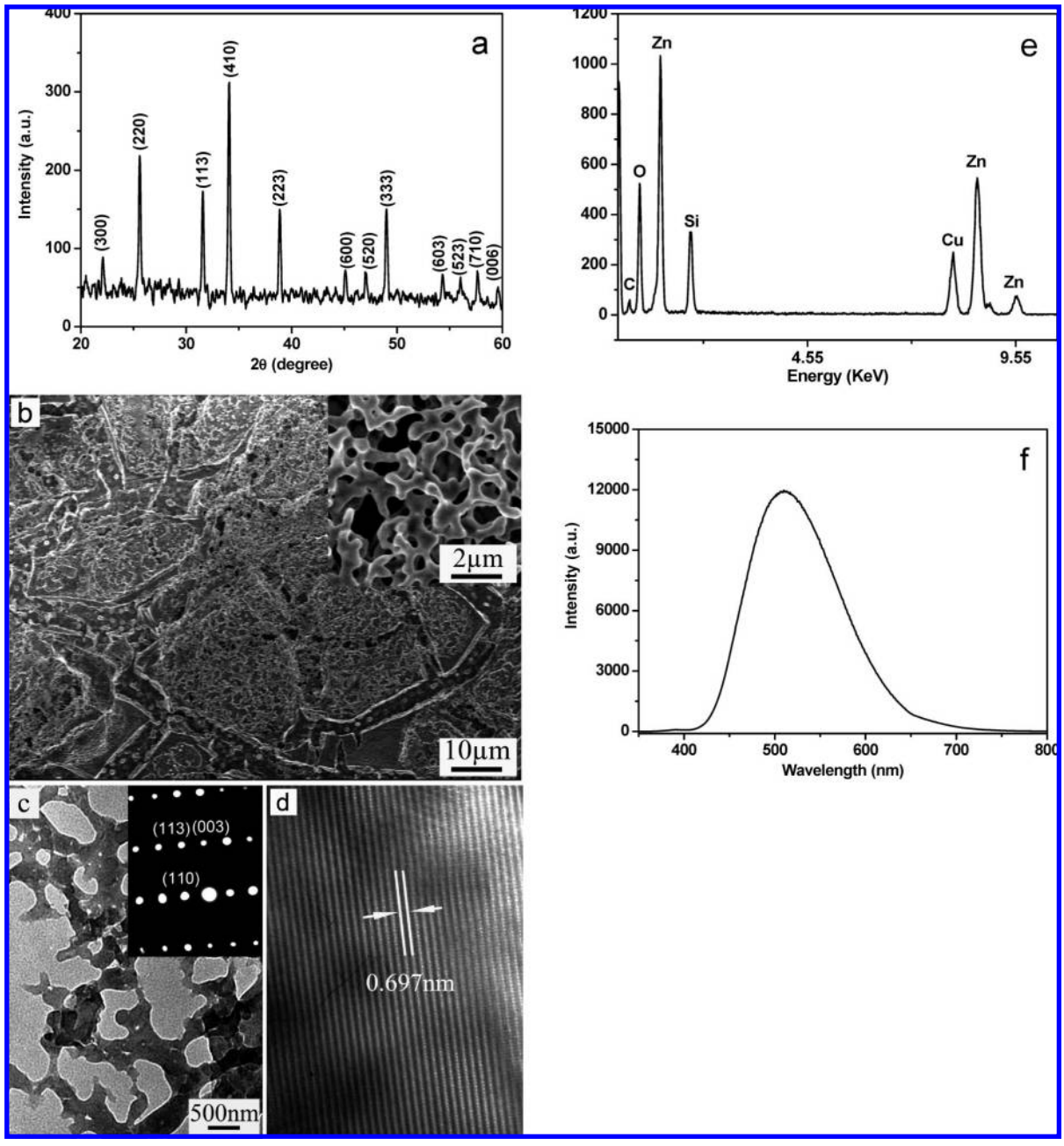

Figure 3. (a) XRD pattern of the Zn_2SiO_4 NWs. (b) SEM image of the Zn_2SiO_4 NWs. The inset shows a close-up view. (c) TEM image and SAED pattern (inset) of the broken fragments of the mesh-like Zn_2SiO_4 NWs. (d) Its corresponding HRTEM image. (e) EDS of the Zn_2SiO_4 nanocrystals. (f) Room-temperature PL spectrum from the Zn_2SiO_4 NWs.

$=N^-$ (the $=N$ energy level as the hole traps), $\equiv Si^0$ (the Si donor energy level), and $\equiv Si^-$ (the Si acceptor energy level), etc. The emission band at 495 nm (2.5 eV) in our experiment might be attributed to the electronic transition of Ec (the conduction-band bottom) $\rightarrow \equiv Si^0$.

3.3. Zn_2SiO_4 NWs Achieved via Evaporating Zn powder and Oxidizing Porous Silicon. Figure 3a shows an XRD pattern of the Zn_2SiO_4 products, which can be indexed to the rhombohedral structure of Zn_2SiO_4 (JCPDS 37-1485). Figure 3b is an SEM image of the Zn_2SiO_4 NWs, and the inset is a close-up view, displaying mesh-like structures, being similar to the previously reported Zn_2SiO_4 NWs.[12] The curved and interconnected Zn_2SiO_4 NWs have diameters about 100−500 nm. Figure 3c is a TEM image taken from broken fragments of the mesh-like Zn_2SiO_4 NWs. The inset in Figure 3c shows a typical SAED pattern taken along the $[\bar{1}100]$ zone axis, and can be indexed to rhombohedral structured Zn_2SiO_4 with (110) and (003). The HRTEM image (Figure 3d) demonstrates that the NWs are well crystallized. The lattice fringe spacing is about 0.697 nm, corresponding to the (110) plane of Zn_2SiO_4. Figure 3e shows the corresponding energy-dispersive X-ray spectroscopy (EDS) of the NWs, revealing that the NWs are composed of Zn, Si, and O, with an atomic ratio about 2:1:4.

The formation of Zn_2SiO_4 NWs can be described as follows. As Zn has a much lower melting point (419 °C), thermal evaporation leads to the sublimation and oxidation of Zn. Then, Zn/ZnO vapor is carried to the low-temperature region by Ar gas and deposits on the surface of PS wafer, resulting in interconnected Zn/ZnO nanocrystals and NWs. Meanwhile, Si−O vapor sublimated from the surface of PS wafer deposits on the ZnO NWs and diffuses into the ZnO lattice, forming a new phase, Zn_2SiO_4.[30] With the prolongation of thermal evaporation, the Zn phase is entirely oxidized and reacts with SiO_x vapor, resulting in mesh-like Zn_2SiO_4 NWs. Figure 3f shows the PL spectrum from the Zn_2SiO_4 NWs

with the excitation wavelength of 275 nm. The emission band at 510 nm can be attributed to Zn_2SiO_4.[30–32]

4. Conclusion

. In summary, we have demonstrated a generic method to fabricate Si-related (β-SiC, α-Si_3N_4, and Zn_2SiO_4) NWs using PS as the Si source. Compared with other Si source materials used previously, a high yield of these Si-related NWs has been achieved. The PL spectra of SiC, Si_3N_4, Zn_2SiO_4 NWs reveal emissions centered at 364 nm, 495 nm, and 510 nm, respectively. The SiC and Si_3N_4 NWs may be used as reinforcing and toughening elements in ceramic, metal, and polymer matrix composites. The Zn_2SiO_4 NWs have potential in future gas sensor and optoelectronic nanodevices. The method reported here might be exploited to fabricate other Si-related NWs.

Acknowledgment. This work was supported by the Natural Science Fund for Distinguished Young Scholars (Grant No. 50525207), the Natural Science Foundation of China (Grant No. 10374092), and the National Basic Research Program of China (Grant No. 2007CB936601).

References

(1) Li, Y. B.; Dorozhkin, P. S.; Bando, Y.; Golberg, D. *Adv. Mater.* **2005**, *17*, 545.
(2) Yang, W.; Araki, H.; Tang, C.; Thaveethavorn, S.; Kohyama, A.; Suzuki, H.; Noda, T. *Adv. Mater.* **2005**, *17*, 1519.
(3) Ye, H.; Titchenal, N.; Gogotsi, Y.; Ko, F. *Adv. Mater.* **2005**, *17*, 1531.
(4) Hu, J. Q.; Lu, Q. Y.; Tang, K. B.; Qian, Y. T.; Zhou, G. E.; Liu, X. M.; Wu, J. X. *Chem. Mater.* **1999**, *11*, 2369.
(5) Bechelany, M.; Brioude, A.; Cornu, D.; Ferro, G.; Miele, P. *Adv. Funct. Mater.* **2007**, *17*, 939.
(6) Zhang, Y. F.; Han, X. D.; Zheng, K.; Zhang, Z.; Zhang, X. N.; Fu, J. Y.; Ji, Y.; Hao, Y. J.; Guo, X. Y.; Wang, Z. L. *Adv. Funct. Mater.* **2007**, *17*, 3435.
(7) Bechelany, M.; Brioude, A.; Stadelmann, P.; Ferro, G.; Cornu, D.; Miele, P. *Adv. Funct. Mater.* **2007**, *17*, 3251.
(8) Chen, I.-W.; Rosenflanz, A. *Nature* **1997**, *389*, 701.
(9) Farjas, J.; Rath, C.; Pinyol, A.; Roura, P.; Bertran, E. *Appl. Phys. Lett.* **2005**, *87*, 192114.
(10) Zhang, L.; Jin, H.; Yang, W.; Xie, Z.; Miao, H.; An, L. *Appl. Phys. Lett.* **2005**, *86*, 061908.
(11) Kroll, P.; Milko, M. *Z. Anorg. Allg. Chem.* **2003**, *629*, 1737.
(12) An, X. H.; Meng, G. W.; Wei, Q.; Zhang, L. D. *J. Cryst. Growth Des.* **2006**, *6*, 1967.
(13) Wei, Q.; Meng, G. W.; Ye, M.; An, X. H.; Hao, Y. F.; Zhang, L. D. *J. Phys. Chem. C* **2007**, *111*, 1924.
(14) Pan, Z.; Lai, H.-L.; Au, F. C. K.; Duan, X.; Zhou, W.; Shi, W.; Wang, N.; Lee, C.-S.; Wong, N.-B.; Lee, S.-T.; Xie, S. *Adv. Mater.* **2000**, *12*, 1186.
(15) Sun, X.-H.; Li, C.-P.; Wong, W.-K.; Wong, N.-B.; Lee, C.-S.; Lee, S.-T.; Teo, B.-K. *J. Am. Chem. Soc.* **2002**, *124*, 14464.
(16) Schroeder, R.; Majewski, L. A.; Grell, M. *Adv. Mater.* **2005**, *17*, 1535.
(17) Meng, G. W.; Zhang, L. D.; Mo, C. M.; Zhang, S. Y.; Qin, Y.; Feng, S. P.; Li, H. J. *J. Mater. Res.* **1998**, *13*, 2533.
(18) Xie, T.; Wu, G. S.; Geng, B. Y.; Jiang, Z.; Yuan, X. Y.; Lin, Y.; Wang, G. Z.; Zhang, L. D. *Appl. Phys. A: Mater. Sci. Process.* **2005**, *80*, 1057.
(19) Yang, Y. J.; Meng, G. W.; Liu, X. Y.; Zhang, L. D. *Angew. Chem., Int. Ed.* **2008**, *47*, 365.
(20) Wang, Z. L.; Dai, Z. R.; Gao, R. P.; Bai, Z. G.; Gole, J. L. *Appl. Phys. Lett.* **2000**, *77*, 3349.
(21) Hao, Y. F.; Meng, G. W.; Wang, Z. L.; Ye, C. H.; Zhang, L. D. *Nano Lett.* **2006**, *6*, 1650.
(22) Stewart, M. P.; Buriak, J. M. *Adv. Mater.* **2000**, *12*, 859.
(23) Gurtner, C.; Wun, A. W.; Sailor, M. J. *Angew. Chem., Int. Ed.* **1999**, *38*, 1966.
(24) Stewart, M. P.; Buriak, J. M. *Angew. Chem., Int. Ed.* **1998**, *37*, 3257.
(25) Pan, Z. W.; Dai, Z. R.; Ma, C.; Wang, Z. L. *J. Am. Chem. Soc.* **2002**, *124*, 1817.
(26) Qin, G. G.; Lin, J.; Duan, J. Q.; Yao, G. Q. *Appl. Phys. Lett.* **1996**, *69*, 1689.
(27) Zou, G. F.; Hu, B.; Xiong, K.; Li, H.; Dong, C.; Liang, J. B.; Qian, Y. T. *Appl. Phys. Lett.* **2005**, *86*, 181901.
(28) Yin, L. W.; Bando, Y.; Zhu, Y. C.; Li, Y. B. *Appl. Phys. Lett.* **2003**, *83*, 3584.
(29) Mo, C. M.; Zhang, L. D.; Xie, C. Y.; Wang, T. *J. Appl. Phys.* **1993**, *73*, 5185.
(30) Wang, X. D.; Summers, C. J.; Wang, Z. L. *Adv. Mater.* **2004**, *16*, 1215.
(31) Xu, C.; Chun, J.; Rho, K.; Kim, D. E. *Nanotechnology* **2005**, *16*, 2808.
(32) Feng, X.; Yuan, X. L.; Sekiguchi, T.; Lin, W. Z.; Kang, J. Y. *J. Phys. Chem. B* **2005**, *109*, 15786.

CG800284U